CORA Cork Open Research Archive
Cartlann Taighde Oscailte Chorcaí

Title	Interplay between competitive and cooperative interactions in a three-player pathogen system
Authors	Pinotti, Francesco;Ghanbarnejad, Fakhteh;Hövel, Philipp;Poletto, Chiara
Publication date	2020-01-22
Original Citation	Pinotti, F., Ghanbarnejad, F., Hövel, P. and Poletto, C. (2020) 'Interplay between competitive and cooperative interactions in a three-player pathogen system', Royal Society Open Science, 7, 190305 (14 pp). doi: 10.1098/rsos.190305
Type of publication	Article (peer-reviewed)
Link to publisher's version	https://royalsocietypublishing.org/doi/pdf/10.1098/rsos.190305 - 10.1098/rsos.190305
Rights	© 2020 The Authors. Published by the Royal Society under the terms of the Creative Commons Attribution License http://creativecommons.org/licenses/by/4.0/, which permits unrestricted use, provided the original author and source are credited. - http://creativecommons.org/licenses/by/4.0/
Download date	2026-11-02 06:04:55
Item downloaded from	https://hdl.handle.net/10468/9884

UCC
University College Cork, Ireland
Coláiste na hOllscoile Corcaigh

ROYAL SOCIETY OPEN SCIENCE

royalsocietypublishing.org/journal/rsos

Research

Cite this article: Pinotti F, Ghanbarnejad F, Hövel P, Poletto C. 2020 Interplay between competitive and cooperative interactions in a three-player pathogen system. *R. Soc. open sci.* **7**: 190305.
http://dx.doi.org/10.1098/rsos.190305

Received: 22 February 2019
Accepted: 13 December 2019

Subject Category:
Ecology, conservation, and global change biology

Subject Areas:
health and disease and epidemiology/theoretical biology/biomathematics

Keywords:
disease ecology, complex networks, multi-pathogen systems, epidemic spreading

Author for correspondence:
Chiara Poletto
e-mail: chiara.poletto@inserm.fr

Electronic supplementary material is available online at https://doi.org/10.6084/m9.figshare.c.4804149.

THE ROYAL SOCIETY PUBLISHING

Interplay between competitive and cooperative interactions in a three-player pathogen system

Francesco Pinotti[1], Fakhteh Ghanbarnejad[2,3,4], Philipp Hövel[2,5] and Chiara Poletto[1]

[1]INSERM, Sorbonne Université, Institut Pierre Louis d'Épidémiologie et de Santé Publique, IPLESP, Paris 75012, France
[2]Institut für Theoretische Physik, Technische Universität Berlin, Hardenbergstraße 36, Berlin 10623, Germany
[3]The Abdus Salam International Centre for Theoretical Physics (ICTP), Trieste, Italy
[4]Physics Department, Sharif University of Technology, PO Box 11165-9161, Tehran, Iran
[5]School of Mathematical Sciences, University College Cork, Western Road, Cork T12 XF62, Republic of Ireland

CP, 0000-0002-4051-1716

In ecological systems, heterogeneous interactions between pathogens take place simultaneously. This occurs, for instance, when two pathogens cooperate, while at the same time, multiple strains of these pathogens co-circulate and compete. Notable examples include the cooperation of human immunodeficiency virus with antibiotic-resistant and susceptible strains of tuberculosis or some respiratory infections with *Streptococcus pneumoniae* strains. Models focusing on competition or cooperation separately fail to describe how these concurrent interactions shape the epidemiology of such diseases. We studied this problem considering two cooperating pathogens, where one pathogen is further structured in two strains. The spreading follows a susceptible-infected-susceptible process and the strains differ in transmissibility and extent of cooperation with the other pathogen. We combined a mean-field stability analysis with stochastic simulations on networks considering both well-mixed and structured populations. We observed the emergence of a complex phase diagram, where the conditions for the less transmissible, but more cooperative strain to dominate are non-trivial, e.g. non-monotonic boundaries and bistability. Coupled with community structure, the presence of the cooperative pathogen enables the coexistence between strains by breaking the spatial symmetry and dynamically creating different ecological niches. These results shed light on ecological mechanisms that may impact the epidemiology of diseases of public health concern.

© 2020 The Authors. Published by the Royal Society under the terms of the Creative Commons Attribution License http://creativecommons.org/licenses/by/4.0/, which permits unrestricted use, provided the original author and source are credited.

1. Introduction

Pathogens do not spread independently. Instead, they are embedded in a larger ecosystem that is characterized by a complex web of interactions among constituent elements. Among ecological forces shaping such ecosystems, pathogen–pathogen interactions have drawn increasing attention during recent years owing to their population-level impact and public health consequences. Recent advances in serological tests and genotyping techniques have improved our reconstruction of pathogen populations where multiple strains co-circulate, often competing owing to cross-protection or mutual exclusion. Examples include tuberculosis [1,2], *Plasmodium falciparum* [3], *Streptococcus pneumoniae* [4,5] and *Staphylococcus aureus* [6,7]. Polymorphic strains can also interact in more complex ways, with both competition and cooperation acting simultaneously, as observed in co-circulating dengue serotypes [8]. While interfering with each other, strains also interact with other pathogens co-circulating in the same population. Tuberculosis [1], human papillomavirus (HPV) [9] and *P. falciparum* [10], for example, appear to be facilitated by human immunodeficiency virus (HIV), whereas *Str. pneumoniae* benefits from some bacterial infections, e.g. *Moraxella catarrhalis*, and is negatively associated with others such as *Sta. aureus* [11,12]. Competition, cooperation and their co-occurrence may fundamentally alter pathogen persistence and diversity, thus calling for a deep understanding of these forces and their quantitative effects on spreading processes.

Mathematical models represent a powerful tool to assess the validity and impact of mechanistic hypotheses about interactions between pathogens or pathogenic strains [13,14]. The literature on competitive interactions is centred on pathogen dominance and coexistence. Several factors were found to affect the ecological outcome of the competition, including co-infection mechanisms [15–18], host age structure [19,20], contact network [21–32] and spatial organization [33–38]. At the same time, models investigating cooperative interactions have driven many research efforts during recent years [39–45]. Cooperation has been found to trigger abrupt transitions between disease extinction and large scale outbreaks along with hysteresis phenomena where the eradication threshold is lower than the epidemic threshold [39,40,43]. These findings were related to the high burden of synergistic infections, e.g. the HIV and tuberculosis co-circulation in many parts of the world. Despite considerable mathematical and computationally heavy research on interacting pathogens, competition and cooperation have been studied mostly separately. Nevertheless, current understandings about these mechanisms taken in isolation may fail to describe the dynamics arising from their joint interplay, where heterogeneous interactions may shape the phase diagram of coexistence/dominance outcome, along with the epidemic prevalence.

Here we studied the simplest possible epidemic situation where these heterogeneous effects are at play. We introduced a three-player model where two pathogens cooperate, and one of the two is structured in two mutually exclusive strains. This mimics a common situation, where e.g. resistant and susceptible strains of *Str. pneumoniae* cooperate with other respiratory infections [11] and allows us to address two important ecological questions:

— how does the interplay between two distinct epidemiological traits, i.e. the transmissibility and the ability to exploit the synergistic pathogen, affect the spreading dynamics? and
— how does the presence of a synergistic infection alter the coexistence between competing strains?

We addressed these questions by providing a characterization of the phase space of dynamical regimes. We tested different modelling frameworks (continuous and deterministic vs. discrete and stochastic) and compared two assumptions regarding population mixing, i.e. homogeneous vs. community structure.

The paper is structured as follows: §2 introduces the main aspects of the three-player model. We provide the results of the deterministic dynamical equations in §3.1, where we present the stability analysis, together with the numerical integration of the equations, to characterize the phase space of the dynamics. The structuring of the population in two communities is analysed in §3.2. In §3.3, we describe the results obtained within a network framework comparing stochastic simulations in an Erdős–Rényi and a random modular network. We discuss the implications of our results in §4.

2. The model

A scheme of the model is depicted in figure 1*a*. We considered the case in which two pathogens, A and B, follow susceptible-infected-susceptible (SIS) dynamics, and we made the simplification that they both have the same recovery rate μ. A and B cooperate in a symmetric way through increased

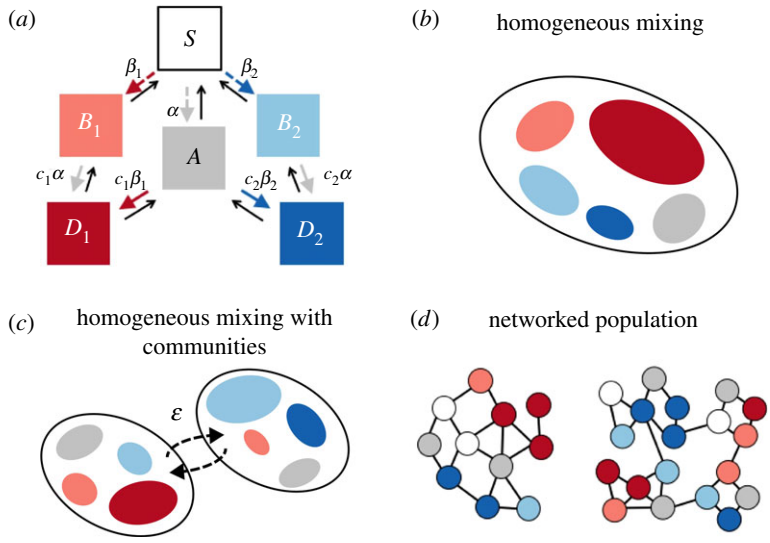


Figure 1. Scheme of the model. (*a*) Compartmental model. Coloured arrows represent transitions occurring owing to infection transmission. Dashed arrows refer to primary infections, while solid arrows refer to secondary ones; transmission parameters are also reported close to each arrow. Black arrows represent recovery transitions. (*b–d*) Schematic representation of the modelling frameworks and population structures considered. (*b*) A homogeneously mixed population (§3.1). (*c*) Two homogeneous populations with across-group mixing ruled by the parameter ε (§3.2); in (*b*),(*c*), colours indicate the infectious density for each compartment. (*d*) Erdős–Rényi and random modular networks (§3.3). Colours indicate the nodes' status.

susceptibility, i.e. a primary infection by one of the two increases the susceptibility to a secondary infection by the other pathogen. We assumed that the cooperative interaction does not affect infectivity, thus doubly infected individuals, i.e. infected with both A and B, transmit both diseases at their respective infection rates. B is structured in two strains, B_1 and B_2, that compete through mutual exclusion (co-infection with B_1 and B_2 is impossible) and differ in epidemiological traits. Specifically, we denoted the infection rates for pathogens A and B_i with α and β_i ($i = 1, 2$), respectively. We introduced the parameters $c_i > 1$ to represent the increased susceptibility after a primary infection. In summary, individuals can be in either one of six states: susceptible (S), singly infected (A, B_i) and doubly infected with both A and B_i. The latter status is denoted by D_i.

To simplify the analytical expressions, we rescaled time by the average infectious period μ^{-1}, which leads to non-dimensional equations. The basic reproductive ratios of each player, $R_0^{(i)} = \beta_i/\mu$ and $R_0^{(A)} = \alpha/\mu$, then become equal to the transmission rates β_i and α, respectively. This implies that the threshold condition β_i, $\alpha > 1$ has to be satisfied in order for the respective player to be able to individually reach an endemic state. Assuming a homogeneously mixed population, the mean-field equations describing the spreading dynamics are:

$$\left.\begin{aligned}
\dot{S} &= A + B_1 + B_2 - \alpha S X_A - \beta_1 S X_1 - \beta_2 S X_2 \\
\dot{B}_1 &= D_1 - B_1 - c_1 \alpha B_1 X_A + \beta_1 S X_1 \\
\dot{B}_2 &= D_2 - B_2 - c_2 \alpha B_2 X_A + \beta_2 S X_2 \\
\dot{A} &= D_1 + D_2 - A + \alpha S X_A - c_1 \beta_1 A X_1 - c_2 \beta_2 A X_2 \\
\dot{D}_1 &= -2D_1 + c_1 \alpha B_1 X_A + c_1 \beta_1 A X_1 \\
\text{and} \quad \dot{D}_2 &= -2D_2 + c_2 \alpha B_2 X_A + c_2 \beta_2 A X_2,
\end{aligned}\right\} \tag{2.1}$$

where the dot indicates a differentiation with respect to time rescaled by μ^{-1}, and quantities S, A, B_i and D_i represent occupation numbers of the compartments divided by the population. The variables X_A, X_i, $i = 1, 2$, indicate the total fractions of individuals carrying A and B_i, respectively, among the singly and doubly infected individuals. They satisfy the equations:

$$\dot{X}_i = X_i \beta_i (S + c_i A) - X_i \tag{2.2a}$$

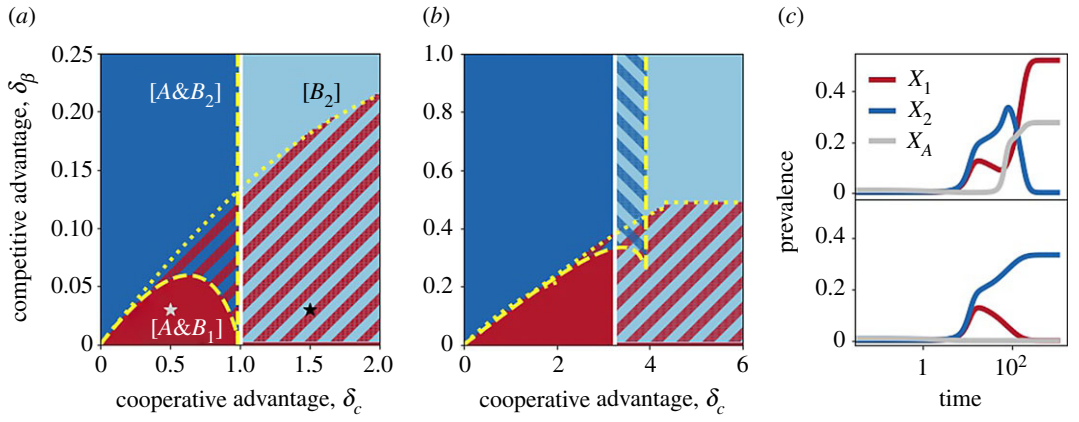


Figure 2. Phase diagram for the well-mixed system. (*a*,*b*) Stable equilibria as a function of δ_β and δ_c for two parameter choices, namely (*a*) $\alpha = 0.6$, $\beta_2 = 1.5$, $c_1 = 4$ and (*b*) $\alpha = 0.8$, $\beta_2 = 1.1$, $c_1 = 7$. The three states $[B_2]$, $[A\&B_2]$ and $[A\&B_1]$ are indicated in light blue, dark blue and red, respectively. Hatched regions correspond to bistable and multi-stable regions. The yellow curves show the analytical boundaries delimiting stability regions for $[A\&B_1]$ and $[A\&B_2]$ (equations (3.2) and (3.3)), while the white one delimits the $[B_2]$'s region (equation (3.1)). Note that for $\delta_c > 3$, 6, for (*a*,*b*), respectively, $c_2 < 1$ and the interaction between B_2 and A ceases to be cooperative. This naturally provides a range for the *x*-axis. In (*b*), β_1 is below one for $\delta_\beta > 0.1$. (*c*) Evolution of total prevalence for A (grey), B_1 (red) and B_2 (blue), considering singly and doubly infected combined. Parameters correspond to the grey and black star markers in (*a*), i.e. $\delta_\beta = 0.03$ and $\delta_c = 0.5$, 1.5 in top and bottom panels, respectively. Dynamical trajectories have been obtained by integrating equations (2.1) with initial conditions: $B_i(t = 0) = 0.001$, $A(t = 0) = 0.01$.

and

$$\dot{X}_A = X_A\alpha(S + c_1B_1 + c_2B_2) - X_A. \tag{2.2b}$$

Without the loss of generality, we considered the case in which the strain B_2 is more transmissible than B_1, i.e. $\delta_\beta = \beta_2 - \beta_1 > 0$. Furthermore, we focused on the more interesting case of trade-off between transmissibility and cooperation to limit the parameter exploration: the less transmissible strain, B_1, is more cooperative, $\delta_c = c_1 - c_2 > 0$. If B_2 is more cooperative, we expect it to win the competition. To summarize, our main assumptions are:

— $\delta_\beta = \beta_2 - \beta_1 > 0$,
— $\delta_c = c_1 - c_2 > 0$,
— $c_i > 1 \qquad i = 1, 2.$

In §3, we will first describe the dynamics arising from the deterministic equation (2.1). We will then consider the case in which the whole population is structured in two groups (figure 1*c*). Finally, we will apply the proposed model to contact networks, where nodes represent individuals and transmission occurs through links, and consider transmission and recovery as stochastic processes. Two types of networks will be tested: Erdős–Rényi and random modular networks (figure 1*d*).

3. Results

3.1. Continuous well-mixed system

We carried out a stability analysis to classify the outcome of the interaction as a function of the difference in strain epidemiological traits, δ_c and δ_β. Specifically, we computed explicit analytical expressions for states' feasibility and stability conditions in several cases. Furthermore, we performed extensive numerical simulations in cases where closed expressions were difficult to obtain. We present the overall behaviour and the main analytical results in this section and we refer to the electronic supplementary material for the detailed calculations. In the following, we will use square brackets to indicate final state configurations in terms of persisting strains, thus $[A\&B_1]$ indicates, for instance, the equilibrium configuration where both A and B_1 persist, while B_2 becomes extinct.

Figure 2*a*,*b* shows the location of stable states with two combinations of α, β_2 and c_1. Results that are obtained for other parameter values are reported in the electronic supplementary material, figure S1. No coexistence was found between B_1 and B_2. In principle, equations (2.1) admit a coexistence equilibrium

$[A\&B_1\&B_2]$. However, this coexistence was always found to be unstable in the numerical simulations. Persistence of A is only possible together with one of the B strains. The equilibrium solution $[A]$ is unfeasible for $\alpha < 1$ and unstable for $\alpha > 1$, unless both reproductive ratios, β_i, are below the epidemic threshold. Because of the assumption $\delta_\beta > 0$, B_2 outcompetes B_1 in absence of A, in agreement with the principle of competitive exclusion. Therefore, the final state $[B_1]$ is always unstable, and persistence of B_1 is possible only in co-circulation with A. On the other hand, B_2 can spread either alone or together with A. Specifically, the $[B_2]$ configuration is feasible for $\beta_2 > 1$. It is stable if and only if $\alpha < \alpha_c$, with

$$\alpha_c = \frac{\beta_2}{c_2(\beta_2 - 1) + 1}. \tag{3.1}$$

This provides a sufficient condition for the persistence of A. Equation (3.1) can be expressed in terms of δ_c, namely $\delta_c > c_1 - (\beta_2 - \alpha)/[\alpha(\beta_2 - 1)]$, which is visualized as the white boundary in figure 2*a*,*b*.

The competition between B_1 and B_2 is governed by the trade-off between transmission and cooperative advantage. This is described by the boundaries of the $[A\&B_i]$ regions that can be traced by combining the feasibility and stability conditions. These boundaries are plotted in figure 2*a*,*b* as dotted and dashed yellow curves for $[A\&B_1]$ and $[A\&B_2]$, respectively. For a solution to be feasible, the densities of all states must be non-negative. For absolute parameter values as in figure 2*a*,*b* we found that this yields the necessary condition $\alpha\beta_i > 4(c_i - 1)/c_i^2$, corresponding to the vertical and horizontal segments. On the other hand, the stability boundary separating $[A\&B_i]$ from any state containing B_j $(j \neq i)$ is given by

$$\beta_j(S^* + c_j A^*) - 1 < 0, \tag{3.2}$$

where S^* and A^* are the equilibrium densities of S and A, respectively, evaluated in the configuration $[A\&B_i]$. The left-hand side of the equation represents the growth rate of the competitor B_j, appearing in equation (2.2*a*), and evaluated in the $[A\&B_i]$ state. Thus, the relation (3.2) expresses the condition for B_j extinction. Expressed in terms of δ_c and δ_β, the conditions become:

$$\left.\begin{aligned} &[A\&B_1]: \frac{\beta_2(c_1 - \delta_c)}{c_1(\beta_2 - \delta_\beta)} + \frac{\beta_2\delta_c}{c_1 - 1}\left(1 - \sqrt{1 - \frac{4(c_1 - 1)}{c_1^2(\beta_2 - \delta_\beta)\alpha}}\right) = 1 \\ \text{and} \quad &[A\&B_2]: \frac{c_1(\beta_2 - \delta_\beta)}{\beta_2(c_1 - \delta_c)} - \frac{\delta_c(\beta_2 - \delta_\beta)}{c_1 - \delta_c - 1}\left(1 - \sqrt{1 - \frac{4(c_1 - \delta_c - 1)}{\beta_2\alpha(c_1 - \delta_c)^2}}\right) = 1. \end{aligned}\right\} \tag{3.3}$$

The intersection among the stability boundaries described above produces a rich state space. For all tested values of α, β_2 and c_1, we found a wide region of the (δ_c, δ_β) space (red-hatched in figure 2*a*,*b*) displaying bistability between the $[A\&B_1]$ state and a B_2-dominant state with either $[B_2]$ or $[A\&B_2]$. In certain cases, bistability can also occur between the $[B_2]$ and $[A\&B_2]$ states (blue-hatched region in figure 2*b*). This has been studied in the past for two cooperating pathogens [43]. We found that the intersection between the latter region and the red-hatched region gives rise to a multi-stable state.

Interestingly, for all tested parameters, we found that the boundary of the $[A\&B_2]$ stability region is not monotonic. As a consequence, for a fixed δ_β, a first transition from the $[A\&B_2]$ state to $[A\&B_1]$ is found for small δ_c values. An increase of δ_c leads to a second boundary with a bistable region, where the dominance of B_1 over B_2 depends on initial conditions. The transition for small δ_c is expected: by increasing B_1's advantage in cooperation, a point is reached beyond which B_1's disadvantage in transmissibility is overcome. On the other hand, the second threshold appears to be counterintuitive. We investigated it more in depth for the case depicted in figure 2*a*. We plotted the infectious population curves as a function of time for each infectious compartment. We compared $\delta_c = 0.5$, which corresponds to the $[A\&B_1]$ stable state (figure 2*c* top), and $\delta_c = 1.5$, which leads to a bistable region (figure 2*c* bottom), where all other parameters are as in figure 2*a*. Figure 2*c* shows that B_1 loses the competition at the beginning. However, when B_2 is sufficiently cooperative with A (top), the rise of B_2 leads to a rise in A that ultimately drives B_1 to dominate. For higher δ_c, the strength of cooperation between B_2 and A is not sufficient. The indirect beneficial effect of B_2 over B_1 is not present (bottom), and B_1 can dominate only if initial conditions are favourable.

In the bistable and multi-stable regions, the outcome of the competition is determined by initial conditions. While a mathematical analysis is complicated owing to the multi-dimensionality of the problem, we gained insights into the basins of attraction by numerically integrating equation (2.1) while exploring different combinations of $B_i(t = 0)$ and $A(t = 0)$. For the bistability between the regions

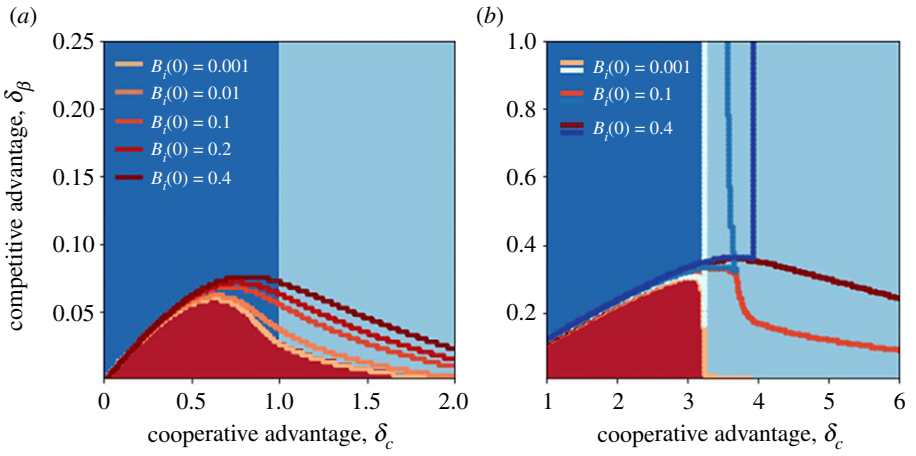


Figure 3. Equilibrium configurations for the well-mixed system. Final outcome obtained by numerically integrating equations (2.1) for $B_i(t=0) = 0.001$, $A(t=0) = 0.01$. (*a*) $\alpha = 0.6$, $\beta_2 = 1.5$, $c_1 = 4$. Boundaries of the $[A\&B_1]$ state for different initial conditions are indicated by red-scale contours. (*b*) $\alpha = 0.8$, $\beta_2 = 1.1$, $c_1 = 7$. Here, the boundaries of the $[A\&B_2]$ are shown (in blue shades), together with the ones of $[A\&B_1]$.

of B_1 and B_2 dominance, we considered the parameter combination of figure 2*a* and shown in figure 3*a* the states that are reached starting from $B_i(t=0) = 0.001$ and $A(t=0) = 0.01$. The bundle of curves with different shades of red (from light to dark) indicates the boundary of the $[A\&B_1]$ equilibrium when $B_1(t=0)$ and $B_2(t=0)$ are equally increased. We found that an increase in B_1's initial infected densities favours the $[A\&B_1]$ state, as expected. Interestingly, however, an increase in $B_1(t=0)$ results in the $[A\&B_1]$ region expanding even when B_2's density increases at the same level. Figure 3*b* shows that a similar behaviour is found when parameters are as in figure 2*b*. In this case, the region $[A\&B_2]$ expands together with the $[A\&B_1]$ one. Thus, increased initial frequencies promote co-circulation between B and A. In the electronic supplementary material, figure S2, we present a deeper exploration of initial conditions, considering the parameter combination of figure 2*a* as an example. We found that an increase in the initial level of A also favours B_1. However, the initial advantage (either in $B_1(0)$ or $A(0)$) that is necessary for B_1 to win against B_2 increases as δ_β increases.

The stability diagrams obtained with several parameter sets, explored in a latin-square fashion, is reported in the electronic supplementary material, figure S1. This shows that increased transmissibility and cooperativity levels enhance the cooperative interaction of B_i strains with A. This results in an increase in the parameter region for which B_1 together with A dominates over B_2. For instance, the comparison between figure 2*d* and *f* shows that, by increasing β_2 from 1.1 to 1.5, the same difference in strain epidemiological traits, δ_c and δ_β, may lead to a switch in dominance from B_2 to B_1.

3.2. Continuous system with communities

We now consider a population that is divided into two communities (cf. figure 1*c*). For simplicity, we assumed that they are of the same size. To differentiate transmission within and across communities, we rescaled the force of infection produced by individuals of a different community by a factor ε, and the force of infection of individuals of the same community by $1-\varepsilon$. We assumed $0 < \varepsilon \leq \frac{1}{2}$ in order to consider the case in which individuals mix more within their community than outside – the limit $\varepsilon = \frac{1}{2}$ corresponds to homogeneous mixing.

Given the high number of variables, a stability analysis is difficult in this case. Still, the dynamics can be reconstructed through numerical integration of the equations. Figure 4 shows the final states with fixed ε, β_2, C_1 and α. Other parameter values are analysed in the electronic supplementary material, figure S3. Figure 4*a–c* compares different seeding configurations, while keeping the initial density of each pathogen/strain to 0.01: (*a*) all strains are seeded in community 1 and community 2 is completely susceptible; (*b*) B_1 is seeded in community 1 while B_2 and A are initially present in community 2 only; and (*c*) B_1 and A are seeded together in community 1, while B_2 is seeded in community 2. In all cases, we found a diagram with a shape similar to figure 3*a*. However, a new region is now present (indicated in black) where all players coexist. This occurs when strains are separated since the beginning—see the electronic supplementary material, figure S4 for additional

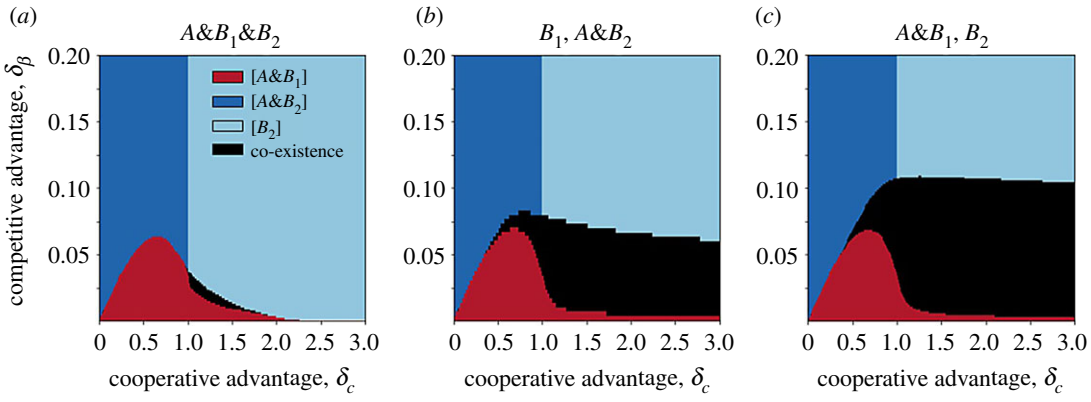


Figure 4. Equilibrium configurations for two interacting communities. Final outcome obtained by numerically integrating the equations when: (*a*) all strains start in the same community (together with *A*); (*b*) B_1 and B_2 start in separate communities, with *A* starting together with B_2; (*c*) *A* starts along with B_1, while B_2 starts separately. Initial density of each pathogen/strain is 0.01. Here $\varepsilon = 0.0002$. Other parameters are as in figure 2*a*.

seeding configurations. Interestingly, however, this also happens for a tiny region of the parameter space, when all strains are seeded together (figure 3*a*), provided that the other community is initially disease-free.

Figure 5 sheds light on the dynamics leading to the outcomes of figure 4. In order to benefit from the cooperative advantage, the B_1 incidence must be above a certain threshold. Figure 5*b*,*c* show that the incidence of *A* remains close to zero, until the incidence of B_1 is sufficiently high. With B_2 seeded on a different community (community 2), the direct interaction between the two strains is delayed by the time necessary for B_2 to reach the community of B_1. For high ε, the delay is short and B_2 reaches community 1 before *A* incidence starts to rise (figure 5*a*). On the other hand, for lower ε, B_1 has enough time to build up a cooperative protection before the arrival of B_2. This makes it resistant to the invader. At intermediate ε, B_1 becomes able to overcome B_2 in community 2. For small ε, strains spread in their origin community independently from one another.

In summary, a decrease in ε increases the region of B_1 persistence (figure 5*d*). However, this may be associated with either B_1 dominance or coexistence. Reducing the values of ε, the region corresponding to the $[A\&B_1]$ state expands first and shrinks later, leaving the place to the coexistence region. This is shown by the non-monotonous change of the $[A\&B_1]$ region in figure 5*e*.

When all strains start in the same community, coexistence is enabled by a segregation mechanism similar to the one described above. In this case, separation occurs during the early stage: B_2 rapidly spreads in the other community owing to its advantage in transmissibility and becomes dominant there (cf. electronic supplementary material, figure S5). This enables coexistence in a parameter region where B_1 would otherwise dominate.

Results described so far were obtained with fixed values of β_2, C_1 and α. Additional parameter choices are shown in the electronic supplementary material, figure S3. Increasing in α was found to enlarge the B_1 dominance region, as in the well-mixed case. In addition, coexistence becomes possible for $\alpha > 1$ in a very small region of the parameter space.

3.3. Spreading on networks

The continuous-deterministic framework analysed so far does not account for stochasticity and for the discrete nature of individuals and their interactions. These aspects may alter the phase diagram and shape the transitions across various regions. We cast our model on a discrete framework in which individuals are represented by nodes in a static network. Possible individual states are still the same as in the mean-field formulation, and infection can spread only between neighbouring nodes. We first considered an Erdős–Rényi graph, where the mixing is homogeneous across nodes. Denoting N the number of nodes and $\bar{k}$ the average degree, the network was built by connecting any two nodes with probability $\bar{k}/(N-1)$. We run stochastic simulations of the dynamics. In order to see the effect of multi-pathogen interactions, we minimized the chance of initial stochastic extinction by infecting a relatively high number of nodes at the beginning: 100 infected for each infectious agent. We then computed the fraction of stochastic simulations ending up in any final state, the average prevalence

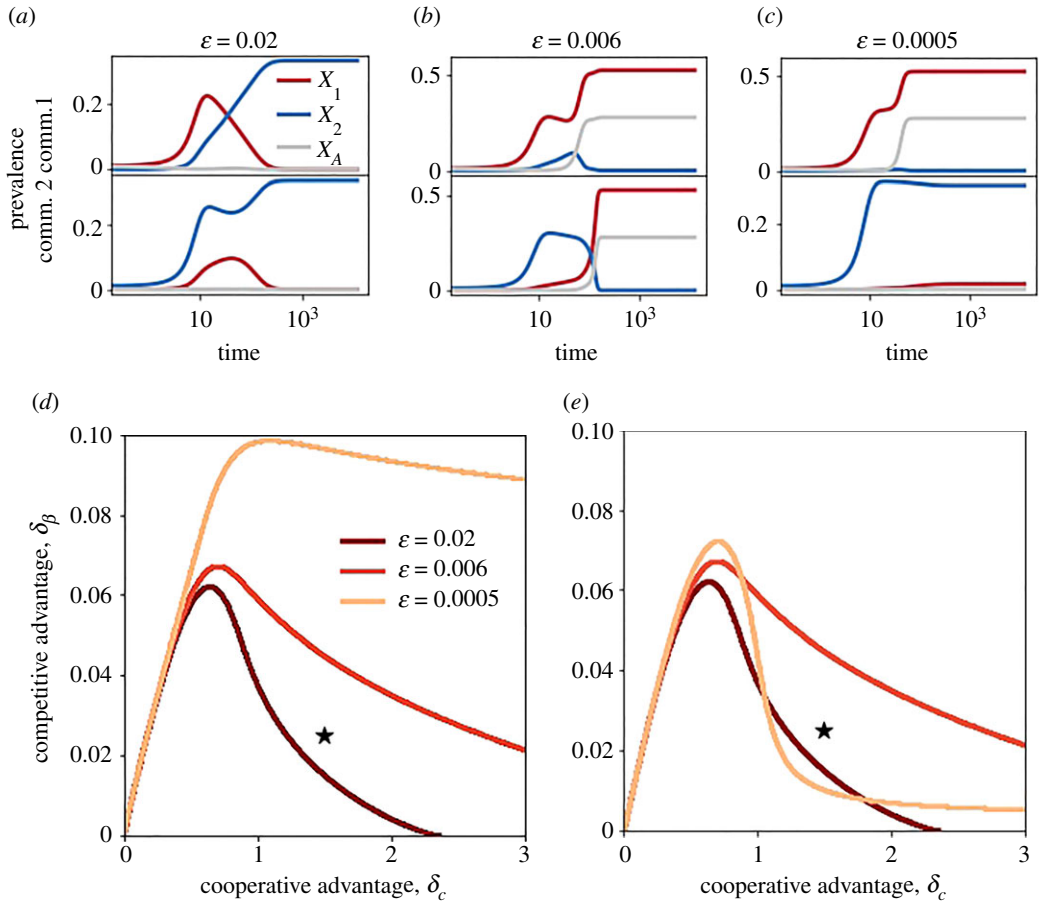


Figure 5. Role of spatial separation for two interacting communities. (*a–c*) Dynamical trajectories within communities 1 and 2 obtained for (*a*) $\varepsilon = 0.02$, (*b*) $\varepsilon = 0.006$ and (c) $\varepsilon = 0.0005$. (*d,e*) Boundaries in the δ_α, δ_β plane delimiting the regions where the dynamics ends up in (*d*) B_1 persistence (i.e. [$A\&B_1$] or full coexistence); (*e*) [$A\&B_1$] state. In all panels, A and B_1 are seeded together into one community, while B_2 is seeded into the other community; the initial density of each species is set to 0.01. Trajectories are obtained by setting $\delta_c = 1.5$, $\delta_\beta = 0.025$ (black star in (*d,e*)). Other parameters are as in figure 2*a*.

for each strain (X_1, X_2) in the final state and the average coexistence time. Additional details on the network model and the simulations are reported in the electronic supplementary material.

The phase diagram of figure 6*a* is similar in many aspects to its continuous deterministic version (figure 3*a*). Three final states are possible, i.e. [B_2], [$A\&B_1$] and [$A\&B_2$] (figure 6*a*). Here, however, the same initial conditions and parameter values can lead to different stochastic trajectories and stationary states. For instance, the red region in the figure corresponds to the case in which the final state [$A\&B_1$] is reached very frequently; however, the dynamic trajectories can also end up in the [$A\&B_2$] or in the [B_2] states. The transitions across the different regions of the diagrams can be very different, as demonstrated by figure 6*b–j*. Figure 6*b–d* shows the effect of varying δ_c at a fixed δ_β. The transition between [$A\&B_2$] and [$A\&B_1$] on the left is sharp. Both the probability of one strain winning over the other and the equilibrium prevalence change abruptly for a critical value of δ_c. Here, the spreading is super-critical for all pathogens: β_1, $\beta_2 > 1$ and c_1, c_2 are sufficiently high to sustain the spread of A. The transition is owing to the trade-off between B_1 and B_2 growth rates. Conversely, the probability of ending up in the [B_2] state rises slowly, driving the gradual transition from the red to the light blue region on the right. This region appears in correspondence of the bistable region of the continuous/deterministic diagram: figure 2. Here, A undergoes a transition from persistence to extinction, driven by the drop in c_2 (electronic supplementary material, figure S6). This critical regime is characterized by enhanced stochastic fluctuations. When δ_c is fixed and δ_β varies, we found a sharp transition (figure 6*e–g*) and a hybrid transition, where the final state probability varies gradually and the equilibrium prevalence (X_1) varies abruptly (figure 6*h–j*).

We concluded by analysing the effect of community structure. Each node was assigned to one among n_C communities, which we assumed for simplicity to have equal size N/n_C, and has a number of open

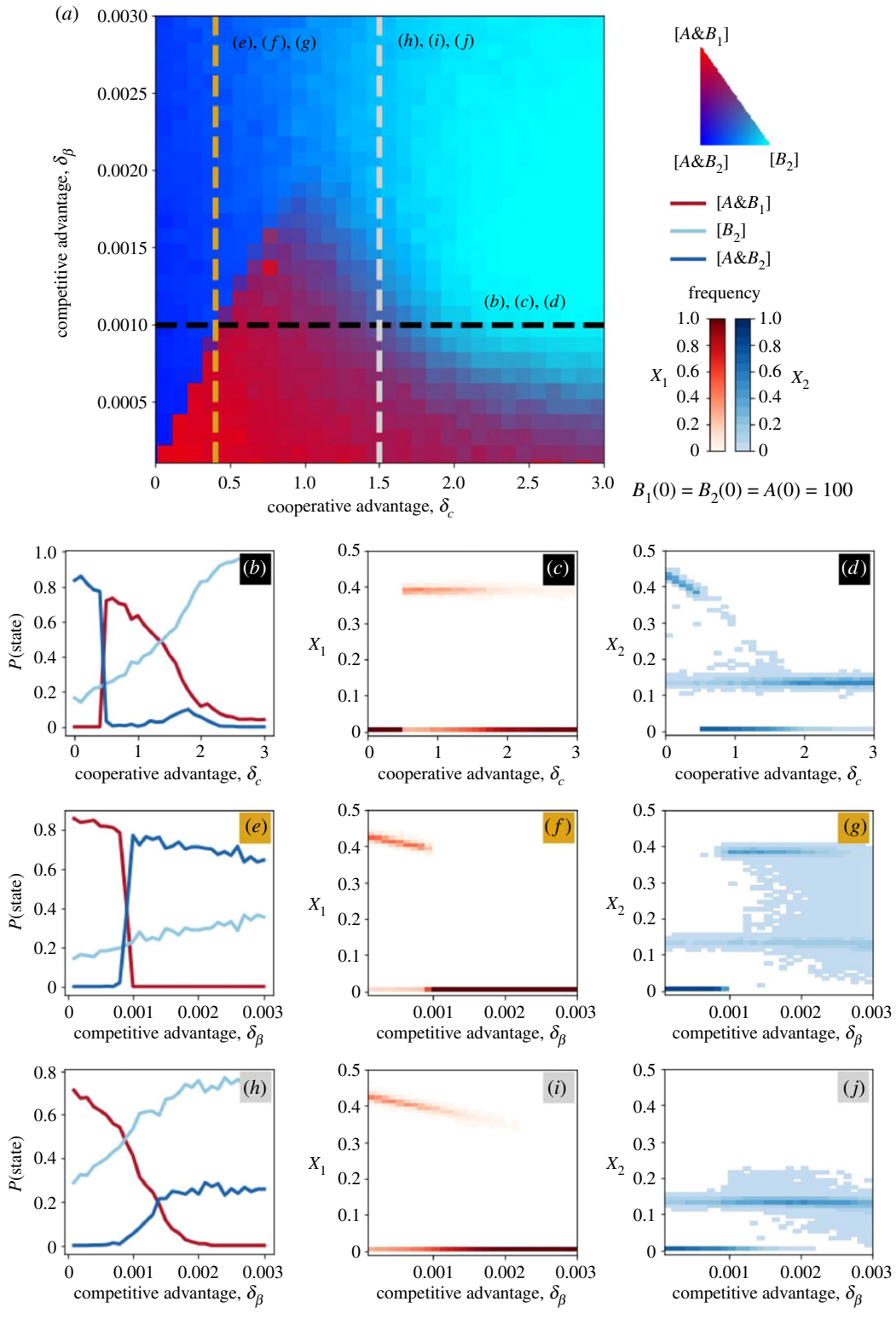


Figure 6. Phase diagram for the Erdős–Rényi network. (*a*) Frequency of stationary states, as obtained in numerical simulations. The colour scale in the legend quantifies the proportion of runs ending in the different states among $[B_2]$, $[A\&B_2]$ and $[A\&B_1]$. Here, the extremes of the colour map correspond to the case in which these states are found in 100% of runs. Initial conditions are shown in the figure. (*b–j*) Equilibrium state probability (left column), and distribution of both B_1's and B_2's prevalence in the final state (middle and right columns respectively) along the dashed lines in (*a*). Specifically: $\delta_\beta = 0.001$ for (*b–d*); $\delta_c = 0.4$ for (*e–g*); $\delta_c = 1.5$ for (*h–j*). For convenience, we reparametrized the model taking the time step as unit of time: $\Delta t = 1$. We set the following parameters' values: $\mu = 0.05$, $\alpha = 0.009$, $\beta_2 = 0.015$, $c_1 = 4$, $N = 20\,000$, $\bar{k} = 4$. Note that in the case of spread on networks, we have $R_0^{(i)} = \beta_i \rho/\mu$ and $R_0^{(A)} = \alpha\rho/\mu$, where ρ is the spectral radius of the adjacency matrix. For the α, β_2 and δ_β values considered in the figure, we have $R_0^{(1)}$, $R_0^{(2)} > 1$.

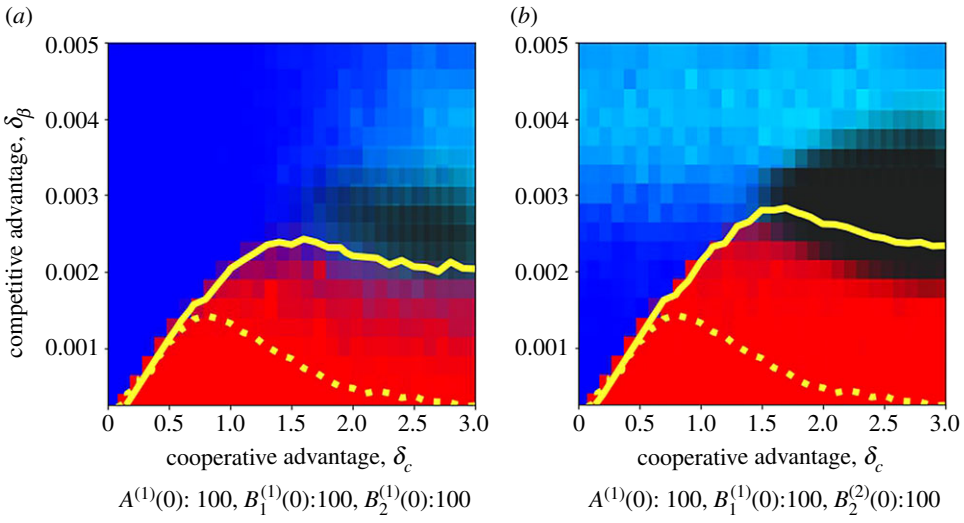


Figure 7. Phase diagram for the random modular network. Frequency of equilibrium configurations, as obtained in the numerical simulations, with (*a*) A, B_1 and B_2 starting in the same community, and (*b*) A and B_1 starting from a different community to B_2. Detailed initial conditions are directly shown on each panel. For each player, the superscript i indicates the community where the infectious are seeded. The colour scale is the same as in figure 6. The frequency of runs for which coexistence of all strains was observed after $T_{\max} = 2 \times 10^6$ time steps is shown with different shades of black. Contour lines representing the 0.5 probability to end up in the $[A\&B_1]$ state are indicated to enable a comparison between the Erdős–Rényi (dashed line) and the random modular network (continuous line). We considered $n_C = 10$ and $\varepsilon = 0.003$. Other parameter values are as in figure 6.

connections drawn from a Poisson distribution with average $\bar{k}$. Links were formed by matching these connections according to an extended configuration model, where a fraction ε of stubs connects nodes of different communities. In this way, the model is the discrete version of the one in §3.2.

Mean-field results remain overall valid. The two plots in figure 7 mirror figure 4*a*,*c* and show a similar behaviour. We find evidence of a coexistence region (in black in the figure), where no extinction is observed during the simulation time frame—here set to 2×10^6 time steps, around two orders of magnitude longer than the time needed to observe strain extinction in the Erdős–Rényi case. Such a region is larger when the two strains are seeded in separated communities (figure 7*b*), but it is still visible when strains start all together (figure 7*a*). Coexistence occurs less frequently in the latter case because it requires strains to reach the separation during the spreading dynamics.

Analogously to the continuous deterministic model, we found that the separation in communities favours the more cooperative strain. The region where B_1 wins is larger compared to the Erdős–Rényi case (as highlighted by the comparison between the dashed and the continuous curves). In addition, the probability of winning is close to one for a large portion of the $[A\&B_1]$ dominance region.

4. Discussion and conclusion

We presented here a theoretical analysis of a three-player system where both competition and cooperation act simultaneously. We have considered two competing strains co-circulating in the presence of another pathogen cooperating with both of them. Strains differ in epidemiological traits, with one strain being more transmissible but less cooperative than its competitor. Through mathematical analyses and computer simulations, we have reconstructed the possible dynamical regimes, quantifying the conditions for dominance of one strain or coexistence. We found that the interplay between competition and cooperation leads to a complex phase diagram whose properties cannot be easily anticipated from previous works that considered competition and cooperation separately.

We showed that it is possible for a more cooperative strain to dominate over a more transmissible one, provided that the difference in transmissibility is not too high. This suggests that the presence of another pathogen (A) might alter the spreading conditions, creating a favourable environment for a strain that would be otherwise less fit. While dominance depends on the difference in epidemiological traits, we found that variations in the absolute cooperation and transmissibility levels may change the hierarchy

between strains—analogously to [15]—with a higher spreading potential of either B_i or A favouring the more cooperative strain.

Interestingly, the cooperative strain can also dominate when A has a sub-critical reproductive ratio ($\alpha < 1$)—when spreading alone—and relies on the synergistic interaction with B strains to persist. The dynamical mechanisms underlying this outcome are complex. We analysed a case with a small difference in cooperativity, and we found that the more transmissible strain, by spreading initially faster, creates the bulk of A infections that in turn favour its competitor. In other words, direct competition for susceptible hosts is not the only force acting between strains: an indirect, beneficial interaction is also at play, mediated by the other pathogen. The dominance outcome is thus the result of the trade-off between these two forces. When the difference in cooperation is higher, two or more stationary configurations are possible. In this scenario, the final outcome is also determined by the initial frequency of each pathogen/strain. We found that, in certain situations, an initial advantage of one strain is able to drive it to dominance. This is in contrast with simpler models of competition, where the final outcome is determined solely by the epidemiological traits. The outcome, however, is also governed by pathogen A that favours the more cooperative strain. Previous works have analysed multistability in two-pathogen models with cooperation in relation to the hysteresis phenomenon, where the eradication threshold is lower than the epidemic one [39,42,43]. A similar mechanism could be at play here. However, the identification of hysteresis loops requires a better reconstruction of the attraction basins. While the numerical work presented here provided some preliminary understanding, a deeper mathematical analysis would be needed in this direction. Multistability is, instead, not present in two-pathogen models with a complete mutual exclusion. This dynamical feature emerges, however, in the more general case where strains are allowed to interact upon co-infection [15].

While we did not find stable coexistence among strains in the well-mixed system, coexistence was possible in presence of community structure. In this case, strains can minimize competition for hosts through segregation. Importantly, spatial separation alone is not sufficient to enable coexistence between two strains, when complete mutual exclusion is assumed. This was already known from previous works which showed that community structure must be combined with some level of heterogeneity across communities to enable coexistence, e.g. a strain-specific adaptation to a population or environment to create an ecological niche [35,37,46–48]. Here, communities are homogeneous and coexistence is the result of the interplay between community structure and presence of the cooperative pathogen. When the two strains are seeded in different communities, their interaction occurs after the time lag necessary for one strain to invade the other community. We found that this interval may allow the resident strain to reach the bulk of infections necessary to fend off the invasion. This mechanism is rooted again in the effect of pathogens' frequencies on strain selective advantage. The drivers of strains' coexistence remain an important problem in disease ecology with applications to both vaccination and emergence of anti-microbial resistance. Within-host and population factors have been studied in the past by several modelling investigations. Notably, while coexistence is not possible in models with complete mutual exclusion, this may be enabled in co-infection models [15–18,49]. Other models have addressed environmental and host population features, such as age structure, contact dynamics and spatial organization [19–21,36]. However, little attention has been dedicated to the effect of an additional co-circulating pathogen. Cobey *et al.* studied the interaction between *Haemophilus influenzae* and *Str. pneumoniae* co-circulating strains [50]. Despite the numerous differences between our model and theirs, their work provides results consistent with ours. Namely, the multi-strain dynamics can be affected by another pathogen.

We simulated the three-player dynamics on networks and we obtained phase diagrams that are similar to the continuous-deterministic counterparts. The discrete/stochastic framework, however, allows for observation of the nature of the phase transitions. Several works recently studied the nature of the epidemic transition for two cooperating pathogens, highlighting differences with the single-pathogen case. Cooperation was found to cause discontinuous transitions where the probability of an outbreak and prevalence change abruptly around a critical value of the transmission rate [40,43], akin to other complex contagion mechanisms such as the ones found in social contagion [51,52]. This phenomenon, however, is sensitive to the network topology, with continuous, discontinuous and hybrid, i.e. continuous in the outbreak probability and discontinuous in the prevalence, transitions observed according to the topology of the network [39,40,42,43,53–55]. Here we found rich dynamics as the impact of stochastic effects. These effects were less important when the difference between strains' epidemiological traits was small. Conversely, for a higher difference in cooperative factor, different outcomes are equally probable. Results presented here are preliminary and limited to two

network configurations. Future work should investigate additional network topologies, e.g. a power-law degree distribution, and further values of the network parameters. In addition, more sophisticated numerical analysis (e.g. scaling analysis) would be needed to better classify the nature of the phase transitions.

Concurrence of inter-species cooperation and intra-species competition is present in many epidemiological situations. Currently, around 90 distinct *Str. pneumoniae* serotypes are known to co-circulate worldwide, despite indirect competition mediated by host immune response [4]. The emergence of antibiotic-resistant strains and the development of vaccines able to target only a subset of strains has motivated extensive research on the drivers of *Str. pneumoniae* ecology [4,5,20]. Strain circulation is facilitated by respiratory infections, e.g. influenza [56,57] and some bacterial infections [11,12]. Cooperative behaviour has also been observed between HIV and infections such as HPV, tuberculosis and malaria [1,9,10,58,59]. This increases the burden of these pathogens and causes public health concern. At the same time, there is evidence that different strains of tuberculosis [2,60], malaria [3] and HPV [61–63] may compete. In particular, multidrug-resistant strains of tuberculosis (MDR-TB) are widely spread, although the acquisition of resistance seems to be associated with a fitness cost [59,64]. The synergistic interaction with HIV could play a role in this emergence and surveillance data suggest a possible convergence between HIV and MDR-TB epidemics in several countries [59]. Our theoretical work highlights ecological mechanisms potentially relevant to these examples. In this regard, an essential aspect of our model is the trade-off between transmissibility and cooperativity in determining strain advantage. Although differences in transmissibility across strains have been documented, e.g. fitness cost of resistance [65], gathering information on strain-specific cooperative advantage remains difficult. The theoretical results illustrated here show the importance of quantifying this component for better describing pathogen ecosystems.

This study also represents the starting point of more complex models where multiple strains are involved and competition and cooperation are acting simultaneously. Patterns of competitive and cooperative interactions could be at play, for instance, among recently emerged pathogens such as Zika virus [66]. Zika virus has emerged in regions where Dengue and Chikungunya viruses are endemic. Observed patterns of sequential monodominance by one arbovirus at a time at a given location suggest competition between these pathogens [67]. Also, considerable effort is currently devoted to characterizing possible positive interactions between Zika virus and HIV [66]. In some cases, different strains of the same pathogen can interact both competitively and cooperatively, as in the case of Dengue [8,14]. Primary Dengue infections are characterized by mild symptoms and grant short-term cross-protection against other serotypes. As cross-immunity wanes over time, however, secondary Dengue infections not only become possible but are also associated with severe illness and with increased virulence.

The examples above involve diseases with varying natural history and time scales and should be modelled with different compartmental models—SIS, susceptible-infected-recovered (SIR), susceptible-infected, susceptible-infected-recovered-susceptible [13]. We decided here to consider two SIS pathogens and the results cannot be readily extended to other models, because the dynamics of disease unfolding alters the outcome of strain interactions. It is important to note, however, that several dynamical properties of competitive and cooperative interactions, such as dominance vs. coexistence [27] and abrupt transitions [68–70], hold for both SIS and SIR.

The model studied here is based on certain simplifications. All pathogens are assumed to have the same recovery rate; moreover, cooperation acts in both directions and the same factors c_i quantify the enhancement in susceptibility when A infection occurs before B_i infection and vice versa. These assumptions may not hold for many synergistic pathogens, especially when cooperative benefits are based on different biological mechanisms. For instance, while HIV increases susceptibility against *P. falciparum*, the latter increases HIV's viral load, thus increasing HIV's virulence rather than host susceptibility to HIV [10,58]. It is likely that, by relaxing these assumptions, our model could exhibit even more complex phase diagrams. Eventually, other aspects of the disease-specific mechanisms and multi-pathogen interactions could affect the results presented here and should be addressed in future works. These include latent infections, which are characteristic, for instance, of tuberculosis [2], partial mutual exclusion among strains [2,6,15,16] or interaction mechanisms other than the ones introduced here (e.g. affecting the infectious period [24]).

In conclusion, we have provided a theoretical study of a dynamical system where both competition and cooperation are at play. We found that a less transmissible and more cooperative strain may dominate; however, the conditions on the parameters for this to happen are non-trivial (non-monotonic) and the outcome critically depends on initial conditions and stochastic effects. When coupled with population structure, the presence of a cooperative pathogen may create the conditions

for multi-strain coexistence by dynamically breaking the spatial symmetry and creating ecological niches. These results provide novel ecological insights and suggest mechanisms that may potentially affect the dynamics of interacting epidemics that are of public health concern.

Data accessibility. The python code used for the mean-field analyses and the C++ code for the stochastic simulations on networks are publicly available at the following link: https://github.com/francescopinotti92/Competition-Cooperation.

Authors' contributions. F.P., F.G., P.H. and C.P. conceived and designed the study. F.P. carried out the analyses. F.P., F.G., P.H. and C.P. analysed the results. F.P., F.G., P.H. and C.P. contributed to the writing of the manuscript and approved the final version.

Competing interests. We declare we have no competing interests.

Funding. F.P. acknowledges support by Pierre Louis Doctoral School of Public Health. F.G. and P.H. acknowledge support by German Academic Exchange Service (DAAD) within the PPP-PROCOPE framework (grant no. 57389088). C.P. and F.P. acknowledge support by the Partenariats Hubert Curien within the PPP-PROCOPE (grant no. 35473TK). F.G. acknowledges partial support by Deutsche Forschungsgemeinschaft (DFG) under the grant GH 176/1-1 (idonate project: 345463468). P.H. acknowledges further support by DFG in the framework of Collaborative Research Center 910 (grant no. SFB910). C.P. acknowledges support from the municipality of Paris through the program Emergence(s).

Acknowledgements. We thank Andrew Keane for helpful discussions that made the manuscript more accessible.

References

1. Tornheim JA, Dooley KE. 2017 Tuberculosis associated with HIV infection. *Microbiol. Spectr.* **5**, TNMI7–0028–2016. (doi:10.1128/microbiolspec.TNM17-0028-2016)
2. Cohen T, Colijn C, Murray M. 2008 Modeling the effects of strain diversity and mechanisms of strain competition on the potential performance of new tuberculosis vaccines. *Proc. Natl Acad. Sci. USA* **105**, 16 302–16 307. (doi:10.1073/pnas.0808746105)
3. Chen K *et al.* 2014 Competition between *Plasmodium falciparum* strains in clinical infections during *in vitro* culture adaptation. *Infect. Genet. Evol.* **24**, 105–110. (doi:10.1016/j.meegid.2014.03.012)
4. Cobey S, Lipsitch M. 2012 Niche and neutral effects of acquired immunity permit coexistence of pneumococcal serotypes. *Science* **335**, 1376–1380. (doi:10.1126/science.1215947)
5. Opatowski L, Varon E, Dupont C, Temime L, van der Werf S, Gutmann L, Boëlle P-Y, Watier L, Guillemot D. 2013 Assessing pneumococcal meningitis association with viral respiratory infections and antibiotics: insights from statistical and mathematical models. *R. Soc. Proc. B* **280**, 20130519. (doi:10.1098/rspb.2013.0519)
6. Obadia T *et al.* 2015 Detailed contact data and the dissemination of *Staphylococcus aureus* in hospitals. *PLoS Comput. Biol.* **11**, e1004170. (doi:10.1371/journal.pcbi.1004170)
7. Donker T *et al.* 2017 Population genetic structuring of methicillin-resistant *Staphylococcus aureus* clone EMRSA-15 within UK reflects patient referral patterns. *Microb. Genomics* **3**, e000113. (doi:10.1099/mgen.0.000113)
8. Reich NG *et al.* 2013 Interactions between serotypes of dengue highlight epidemiological impact of cross-immunity. *J. R. Soc. Interface* **10**, 20130414. (doi:10.1098/rsif.2013.0414)
9. Looker KJ, Rönn MM, Brock PM, Brisson M, Drolet M, Mayaud P, Boily M-C. 2018 Evidence of synergistic relationships between HIV and human papillomavirus (HPV): systematic reviews and meta-analyses of longitudinal studies of HPV acquisition and clearance by HIV status, and of HIV acquisition by HPV status. *J. Int. AIDS Soc.* **21**, e25110. (doi:10.1002/jia2.25110)
10. Cohen C, Karstaedt A, Frean J, Thomas J, Govender N, Prentice E, Dini L, Galpin J, Crewe-Brown H. 2005 Increased prevalence of severe malaria in HIV-infected adults in South Africa. *Clin. Infect. Dis.* **41**, 1631–1637. (doi:10.1086/498023)
11. Bosch AATM, Biesbroek G, Trzcinski K, Sanders EAM, Bogaert D. 2013 Viral and bacterial interactions in the upper respiratory tract. *PLoS Pathog.* **9**, e1003057. (doi:10.1371/journal.ppat.1003057)
12. Dunne EM, Smith-Vaughan HC, Robins-Browne RM, Mulholland EK, Satzke C. 2013 Nasopharyngeal microbial interactions in the era of pneumococcal conjugate vaccination. *Vaccine* **31**, 2333–2342. (doi:10.1016/j.vaccine.2013.03.024)
13. Keeling MJ, Rohani P. 2008 *Modeling infectious diseases in humans and animals*. Princeton, NJ: Princeton University Press.
14. Shrestha S, King AA, Rohani P. 2011 Statistical inference for multi-pathogen systems. *PLoS Comput. Biol.* **7**, e1002135. (doi:10.1371/journal.pcbi.1002135)
15. Gjini E, Madec S. 2017 A slow-fast dynamic decomposition links neutral and non-neutral coexistence in interacting multi-strain pathogens. *Theor. Ecol.* **10**, 129–141. (doi:10.1007/s12080-016-0320-1)
16. Sofonea MT, Alizon S, Michalakis Y. 2015 From within-host interactions to epidemiological competition: a general model for multiple infections. *Phil. Trans. R. Soc. B* **370**, 20140303. (doi:10.1098/rstb.2014.0303)
17. Alizon S. 2013 Co-infection and super-infection models in evolutionary epidemiology. *Interface Focus* **3**, 20130031. (doi:10.1098/rsfs.2013.0031)
18. Alizon S, de Roode JC, Michalakis Y. 2013 Multiple infections and the evolution of virulence. *Ecol. Lett.* **16**, 556–567. (doi:10.1111/ele.12076)
19. Martcheva M, Pilyugin SS, Holt RD. 2007 Subthreshold and superthreshold coexistence of pathogen variants: the impact of host age-structure. *Math. Biosci.* **207**, 58–77. (doi:10.1016/j.mbs.2006.09.010)
20. Cobey S, Baskerville EB, Colijn C, Hanage W, Fraser C, Lipsitch M. 2017 Host population structure and treatment frequency maintain balancing selection on drug resistance. *J. R. Soc. Interface* **14**, 20170295. (doi:10.1098/rsif.2017.0295)
21. Eames KTD, Keeling MJ. 2006 Coexistence and specialization of pathogen strains on contact networks. *Am. Nat.* **168**, 230–241. (doi:10.1086/505760)
22. Miller JC. 2013 Co-circulation of infectious diseases on networks. *Phys. Rev. E Stat. Nonlin. Soft Matter Phys.* **87**, 060801. (doi:10.1103/PhysRevE.87.060801)
23. Sahneh FD, Scoglio C. 2014 Competitive epidemic spreading over arbitrary multilayer networks. *Phys. Rev. E* **89**, 062817. (doi:10.1103/PhysRevE.89.062817)
24. Sanz J, Xia CY, Meloni S, Moreno Y. 2014 Dynamics of interacting diseases. *Phys. Rev. X* **4**, 041005.
25. Li J, Ma Z, Blythe SP, Castillo-Chavez C. 2003 Coexistence of pathogens in sexually-transmitted disease models. *J. Math. Biol.* **47**, 547–568. (doi:10.1007/s00285-003-0235-5)
26. Chai C, Jiang J. 2011 Competitive exclusion and coexistence of pathogens in a homosexually-transmitted disease model. *PLoS ONE* **6**, e16467. (doi:10.1371/journal.pone.0016467)
27. Karrer B, Newman MEJ. 2011 Competing epidemics on complex networks. *Phys. Rev. E* **84**, 036106. (doi:10.1103/PhysRevE.84.036106)
28. Masuda N, Konno N. 2006 Multi-state epidemic processes on complex networks. *J. Theor. Biol.* **243**, 64–75. (doi:10.1016/j.jtbi.2006.06.010)
29. Leventhal GE, Hill AL, Nowak MA, Bonhoeffer S. 2015 Evolution and emergence of infectious

diseases in theoretical and real-world networks. *Nat. Commun.* **6**, 6101. (doi:10.1038/ncomms7101)

30. Buckee CO, Koelle K, Mustard MJ, Gupta S. 2004 The effects of host contact network structure on pathogen diversity and strain structure. *Proc. Natl Acad. Sci. USA* **101**, 10 839–10 844. (doi:10.1073/pnas.0402000101)
31. Pinotti F, Boëlle PY, Poletto C. 2019 Host contact dynamics shapes richness and dominance of pathogen strains. *PLoS Comput. Biol.* **15**, e1006530. (doi:10.1371/journal.pcbi.1006530)
32. Soriano-Paños D, Ghanbarnejad F, Meloni S, Gómez-Gardeñes J. 2019 Markovian approach to tackle the interaction of simultaneous diseases. *Phys. Rev. E* **100**, 062308. (doi:10.1103/PhysRevE.100.062308)
33. Poletto C, Meloni S, Colizza V, Moreno Y, Vespignani A. 2013 Host mobility drives pathogen competition in spatially structured populations. *PLoS Comput. Biol.* **9**, e1003169. (doi:10.1371/journal.pcbi.1003169)
34. Poletto C, Meloni S, Van Metre A, Colizza V, Moreno Y, Vespignani A. 2015 Characterising two-pathogen competition in spatially structured environments. *Sci. Rep.* **5**, 7895. (doi:10.1038/srep07895)
35. Allen LJ, Kirupaharan N, Wilson SM. 2004 SIS epidemic models with multiple pathogen strains. *J. Differ. Equ. Appl.* **10**, 53–75. (doi:10.1080/10236190310001603680)
36. Buckee C, Danon L, Gupta S. 2007 Host community structure and the maintenance of pathogen diversity. *Proc. R. Soc. B* **274**, 1715–1721. (doi:10.1098/rspb.2007.0415)
37. Wu Y, Tuncer N, Martcheva M. 2016 Coexistence and competitive exclusion in an SIS model with standard incidence and diffusion. *Discrete Contin. Dyn. Syst. B* **22**, 1167. (doi:10.3934/dcdsb.2017057)
38. Lion S, Gandon S. 2016 Spatial evolutionary epidemiology of spreading epidemics. *Proc. Biol. Sci.* **283**, 20161170. (doi:10.1098/rspb.2016.1170)
39. Cai W, Chen L, Ghanbarnejad F, Grassberger P. 2015 Avalanche outbreaks emerging in cooperative contagions. *Nat. Phys.* **11**, 936–940. (doi:10.1038/nphys3457)
40. Hébert-Dufresne L, Althouse BM. 2015 Complex dynamics of synergistic coinfections on realistically clustered networks. *Proc. Natl Acad. Sci. USA* **112**, 10 551–10 556. (doi:10.1073/pnas.1507820112)
41. Lee D, Choi W, Kértesz J, Kahng B. 2017 Universal mechanism for hybrid percolation transitions. *Sci. Rep.* **7**, 5723. (doi:10.1038/s41598-017-06182-3)
42. Cui PB, Colaiori F, Castellano C. 2017 Mutually cooperative epidemics on power-law networks. *Phys. Rev. E* **96**, 022301. (doi:10.1103/physreve.96.022301)
43. Chen L, Ghanbarnejad F, Brockmann D. 2017 Fundamental properties of cooperative contagion processes. *New J. Phys.* **19**, 103041. (doi:10.1088/1367-2630/aa8bd2)
44. Rodríguez JP, Liang YH, Huang YJ, Juang J. 2018 Diversity of hysteresis in a fully cooperative coinfection model. *Chaos* **28**, 023107. (doi:10.1063/1.4996807)
45. Rodríguez JP, Ghanbarnejad F, Eguíluz VM. 2017 Risk of coinfection outbreaks in temporal networks: a case study of a hospital contact network. *Front. Phys.* **5**, 46. (doi:10.3389/fphy.2017.00046)
46. Feng Z, Liu R, Qiu Z, Rivera J, Yakubu AA. 2011 Coexistence of competitors in deterministic and stochastic patchy environments. *J. Biol. Dyn.* **5**, 454–473. (doi:10.1080/17513758.2010.535126)
47. Qiu Z, Kong Q, Li X, Martcheva M. 2013 The vector-host epidemic model with multiple strains in a patchy environment. *J. Math. Anal. Appl.* **405**, 12–36. (doi:10.1016/j.jmaa.2013.03.042)
48. Lin KH, Lou Y, Shih CW, Tsai TH. 2014 Global dynamics for two-species competition in patchy environment. *Math. Biosci. Eng.* **11**, 947–970. (doi:10.3934/mbe.2014.11.947)
49. Gjini E, Valente C, Sa-Leao R, Gomes MG. 2016 How direct competition shapes coexistence and vaccine effects in multi-strain pathogen systems. *J. Theor. Biol.* **388**, 50–60. (doi:10.1016/j.jtbi.2015.09.031)
50. Cobey S, Lipsitch M. 2013 Pathogen diversity and hidden regimes of apparent competition. *Am. Nat.* **181**, 12–24. (doi:10.1086/668598)
51. Gómez-Gardeñes J, Lotero L, Taraskin SN, Pórez-Reche FJ. 2016 Explosive contagion in networks. *Sci. Rep.* **6**, 19767. (doi:10.1038/srep19767)
52. Dodds PS, Watts DJ. 2004 Universal behavior in a generalized model of contagion. *Phys. Rev. Lett.* **92**, 218701. (doi:10.1103/PhysRevLett.92.218701)
53. Wang W, Liu QH, Liang J, Hu Y, Zhou T. 2019 Coevolution spreading in complex networks. arXiv: 1901.02125. See http://arxiv.org/abs/1901.02125 [physics].
54. Rodríguez JP, Ghanbarnejad F, Eguíluz VM. 2019 Particle velocity controls phase transitions in contagion dynamics. *Sci. Rep.* **9**, 1–9. (doi:10.1038/s41598-018-37186-2)
55. Choi W, Lee D, Kertész J, Kahng B. 2018 Two golden times in two-step contagion models: a nonlinear map approach. *Phys. Rev. E* **98**, 012311. (doi:10.1103/PhysRevE.98.012311)
56. Shrestha S, Foxman B, Weinberger DM, Steiner C, Viboud C, Rohani P. 2013 Identifying the interaction between influenza and pneumococcal pneumonia using incidence data. *Sci. Transl. Med.* **5**, 191ra84. (doi:10.1126/scitranslmed.3005982)
57. Opatowski L, Baguelin M, Eggo RM. 2018 Influenza interaction with cocirculating pathogens and its impact on surveillance, pathogenesis, and epidemic profile: a key role for mathematical modelling. *PLoS Pathog.* **14**, e1006770. (doi:10.1371/journal.ppat.1006770)
58. Abu-Raddad LJ, Patnaik P, Kublin JG. 2006 Dual infection with HIV and malaria fuels the spread of both diseases in sub-Saharan Africa. *Science* **314**, 1603–1606. (doi:10.1126/science.1132338)
59. Wells CD, Cegielski JP, Nelson LJ, Laserson KF, Holtz TH, Finlay A, Castro KG, Weyer K. 2007 HIV infection and multidrug-resistant tuberculosis: the perfect storm. *J. Infect. Dis.* **196**, Suppl 1 S86–S107. (doi:10.1086/518665)
60. Dowdy DW, Dye C, Cohen T. 2013 Data needs for evidence-based decisions: a tuberculosis modeler's 'wish list'. *Int. J. Tuberc. Lung Dis.* **17**, 866–877. (doi:10.5588/ijtld.12.0573)
61. Pons-Salort M, Letort V, Favre M, Heard I, Dervaux B, Opatowski L, Guillemot D. 2013 Exploring individual HPV coinfections is essential to predict HPV-vaccination impact on genotype distribution: a model-based approach. *Vaccine* **31**, 1238–1245. (doi:10.1016/j.vaccine.2012.11.098)
62. Gray P *et al.* 2019 Occurrence of human papillomavirus (HPV) type replacement by sexual risk-taking behaviour group: post-hoc analysis of a community randomized clinical trial up to 9 years after vaccination (IV). *Int. J. Cancer* **145**, 785–796. (doi:10.1002/ijc.32189)
63. Murall CL, McCann KS, Bauch CT. 2014 Revising ecological assumptions about human papillomavirus interactions and type replacement. *J. Theor. Biol.* **350**, 98–109. (doi:10.1016/j.jtbi.2013.12.028)
64. Gagneux S. 2009 Fitness cost of drug resistance in *Mycobacterium tuberculosis*. *Clin. Microbiol. Infect.* **15**, 66–68. (doi:10.1111/j.1469-0691.2008.02685.x)
65. Melnyk AH, Wong A, Kassen R. 2015 The fitness costs of antibiotic resistance mutations. *Evol. Appl.* **8**, 273–283. (doi:10.1111/eva.12196)
66. Rothan HA, Bidokhti MR, Byrareddy SN. 2018 Current concerns and perspectives on Zika virus co-infection with arboviruses and HIV. *J. Autoimmun.* **89**, 11–20. (doi:10.1016/j.jaut.2018.01.002)
67. Magalhaes T *et al.* 2017 Zika virus displacement by a chikungunya outbreak in Recife, Brazil. *PLoS Negl. Trop. Dis.* **11**, e0006055. (doi:10.1371/journal.pntd.0006055)
68. Grassberger P, Chen L, Ghanbarnejad F, Cai W. 2016 Phase transitions in cooperative coinfections: simulation results for networks and lattices. *Phys. Rev. E* **93**, 042316. (doi:10.1103/PhysRevE.93.042316)
69. Chen L, Ghanbarnejad F, Cai W, Grassberger P. 2013 Outbreaks of coinfections: the critical role of cooperativity. *EPL* **104**, 50001. (doi:10.1209/0295-5075/104/50001)
70. Zarei F, Moghimi-Araghi S, Ghanbarnejad F. 2019 Exact solution of generalized cooperative susceptible-infected-removed (SIR) dynamics. *Phys. Rev. E* **100**, 012307. (doi:10.1103/PhysRevE.100.012307)